Near Surface Geophysics, 2011, **9**, xxx-xxx doi:10.3997/1873-0604.2011030

Geotechnical characterization of a river dyke by surface waves

Lutz Karl[1*], Thomas Fechner[1], Mattias Schevenels[2], Stijn François[2] and Geert Degrande[2]

[1] *Geotomographie GmbH, Am Tonnenberg 18, 56567 Neuwied, Germany*
[2] *Department of Civil Engineering, K.U.Leuven, Kasteelpark Arenberg 40, 3001 Leuven, Belgium*

Received July 2008, revision accepted June 2011

ABSTRACT

The need for effective and reliable methods to survey and monitor the structure of earth-fill dams recently became pressing in light of the increasing number of flood events in central Europe. Among geophysical techniques, dam imaging using electrical resistivity methods is applied in most cases. Occasionally, ground-penetrating radar is applied in the framework of the search for subsurface facilities. Seismic methods are rarely used.

This paper focuses on the multichannel analysis of the surface waves (MASW) method to determine dynamic soil properties and aims to extend its application field to dyke and dam structures. The standard processing procedure of the MASW assumes a flat free surface of infinite extension. The flat surfaces of a dyke, in contrast, are in the order of 1–10 times smaller than the wavelengths in the soil; disturbing side reflections will occur. Even though MASW has already been applied on a few dyke sites, the effect of such an obvious breach of preconditions needs to be studied before the method can be recommended.

In this paper the influences of the dyke's topography on the test results are studied by means of a numerical analysis. Typical cross-sections are modelled using 2.5D finite and boundary elements. The results of models taking the topography into account are compared with models neglecting the topography. The differences are evaluated on the level of the dispersion curves and for one cross-section on the level of the S-wave velocity. They were found to be insignificant for dykes with a width-to-height ratio larger than four.

A testing campaign was conducted providing the chance to collect experience in the practical use of the MASW method on dykes. Test results obtained at two test sites are selected and compared to the results of borehole logs and cone penetration tests. A remarkable relation between the S-wave velocity and the consistency of the clay sealing was found at one site; a distinct positive correlation to the measured cone tip resistances was achieved on the other test site. Valuable information on the composition of the dyke body and base could be obtained but the resolution of the method to identify small areas of inhomogeneity should not be overestimated.

INTRODUCTION

Most river dykes in central Europe were built many decades or even hundreds of years ago. Knowledge of the internal structure of dykes has very frequently been lost by the process of time. If original construction or even as-built drawings are available, it is in most cases not certain up to what extent this information is still representative of the current state. Historical floods, reinforcement measures, traffic and agricultural use may have significantly changed the geometry and structure of the dyke. However, reliable geotechnical parameters of the dyke material are required for the verification of stability. The importance of a continuous observation of dyke stability became obvious in the light of recent flood events in central Europe, such as the Elbe flood of 2002.

Survey campaigns initiated by the dyke authorities focus in general on geotechnical parameters obtained *in situ* by the standard penetration and cone penetration tests, or in the laboratory based on borehole samples. A disadvantage of these tests is their selective character. An extensive number of tests are required to cover a dyke sufficiently. On the other hand, most non-destructive geophysical methods are able to survey large areas effectively but they lack in general a direct functional relationship between the geophysical and the geotechnical parameters.

* lkarl@geotomographie.de

However, in principle, site specific correlation can fill in the gap.

The imaging of electrical resistivity is the most common geophysical method applied on dykes. Profiles along the dyke axis but also perpendicular to the axis can be measured. The resistivity correlates directly to the water content and the saturation of the ground. Conclusions on the type of soil can be drawn based on site specific correlations if borehole profiles are available. Tuyen *et al.* (2000), Donié *et al.* (2007) and Henning *et al.* (2005) provided additional information on dyke specific problems of the method by means of extensive case studies.

Ground-penetrating radar (GPR) is applied on dykes in order to detect subsurface facilities embedded in the dyke. The penetration of the method is often limited to a very shallow range due to the high clay content of the material. Occasionally and listed for completeness, geophysical borehole logging, electromagnetic methods (Fauchard and Mériaux 2007), infra-red surface temperature mapping (Tuyen *et al.* 2000), complex resistivity sounding, IP (induced polarization) and self potential methods are used under specific conditions.

Seismic methods, such as seismic refraction or seismic reflection, are only rarely considered for the survey of dykes since the finite dimensions of the dyke body can cause disturbing reflections in the gathered data. These are difficult to handle during processing. However, seismic velocities are directly related to the dynamic stiffness of the material, expressed as dynamic shear and Young's modulus, which are important mechanical parameters for the recognition of soil layers. In the field of geotechnical engineering, huge research effort is spent on the correlation of the S-wave velocity to parameters obtained from standard geotechnical tests. Site specific but also more general correlations exist to the porosity, the plasticity index, to the shear modulus at higher strains and also to *in situ* tests such as cone penetration, standard penetration, dilatometer and pressure meter tests, for instance reported in Kramer (1996). Correlations to the shear parameters are obtained for very few exceptional cases. The dynamic shear modulus alone gains increasing importance for the verification of the earthquake safety of earth-fill dams.

Among the seismic methods the multichannel analysis of surface waves (MASW), based on the velocity of the Rayleigh wave, is the most effective method for the determination of S-wave profiles. However, the MASW method is commonly applied to sites with a flat free surface only and the solution of the inverse problem is based on the assumption that the subgrade can be modelled as a layered elastic half-space. In case the method is applied on an elevated topography such as a dyke, the pertinent question is if the layered half-space model needs to be modified in order to incorporate the effects of reflections from the boundaries.

Despite this unanswered question, the MASW had already been applied on dykes by other authors, for instance Lane *et al.* (2008). Min and Kim (2006) studied the wave propagation on dam-like structures using a 3D finite difference elastic wave model. They focused on large earth-fill dams with heights in the order of tens of metres. The findings of the finite difference model of a homogeneous and a horizontally layered cross-section were compared with the results from the layered half-space model. The comparison was done on the level of the dispersion curve of the fundamental mode and a good agreement was obtained. However, based on several calculations on a cross-section containing a clay core, the authors concluded that the 1D layered half-space model is not applicable for an inversion. The clay core was placed in the centre of the dam and outcropped at the crest. Stiffer soil formed the main dam body at both sides of the core. The dispersion curve computed by the 3D model was influenced by the properties of the main dam body and the central core. On the contrary, the dispersion curve based on a 1D forward model cannot represent a situation with such an abrupt lateral stiffness change in close proximity to the vertical survey plane since the lateral material properties have to be *a priori* invariant for such a model. Therefore, the authors recommend instead the use of the 3D model for inversion.

Surface wave methods were also applied to structures similar to river dykes. Gunn *et al.* (2006) for instance used the continuous surface wave method for the measurement of the dynamical stiffness of railway embankments.

This paper attempts to provide new insights on MASW surveying of dykes by means of an application oriented numerical study. For the numerical study, dispersion curves of the Rayleigh wave are calculated based on common river dyke geometries and are compared with the results of a standard forward calculation for flat surfaces. Conclusions for a field testing procedure are drawn. A MASW survey campaign on two river dykes in Germany is described. The 2D sections of S-wave velocities obtained are related to available information from borehole logs and the cone penetration test. Finally, a comparison is made between an experimental dispersion curve and the modelled dispersion curves for the flat and topography models. The resulting S-wave profiles are compared.

THE SURFACE WAVE METHOD

The analysis of surface waves uses the properties of elastic waves bounded to the presence of a free surface, such as the soil-air interface. In most cases only waves of the Rayleigh type resulting from a superposition of P- and SV-waves are considered. The elliptical particle motion of these waves is constrained to the vertical plane agreeing with the direction of propagation. The penetration depth depends on the wavelength of the Rayleigh wave: longer wavelengths penetrate deeper than shorter waves. Since the phase velocity of the waves is a direct function of the dynamic stiffness, particularly of the shear stiffness and the density of the material in the penetration zone, Rayleigh waves show a dispersive behaviour. The function between phase velocity and frequency, i.e., the dispersion curve, contains information about the soil layering. Depending on the site stratification, the Rayleigh wave can travel at the same time in different modes, i.e., at a single frequency more than one discrete phase velocity can be measured. The different propagation modes are

numbered according to their phase velocity. The mode with the lowest number is called the fundamental mode.

Stokoe and Nazarian (1983) and Nazarian *et al.* (1983) introduced a procedure for surface wave processing to generate 1D S-wave profiles called spectral analysis of surface waves (SASW), now widely applied to many geotechnical projects. The experimental set-up consists of an active pulse source like a sledge hammer or weight drop and two surface receivers. The phase velocity is derived from the cross-power spectrum between the receiver signals.

Later work focuses on the improvement of the mode identification by applying frequency wavenumber techniques and linear arrays of receivers (Al-Hunaidi 1996; Park *et al.* 1999; Xia *et al.* 1999). Approaches applying multiple receivers are summarized as multichannel analysis of surface wave (MASW) methods and accelerate the test progression significantly. The whole MASW set-up can be shifted along lines and shots can be repeated every few metres. If the receivers are mounted to a land streamer the array can even be towed to a vehicle. Even though the result of a single shot is still only a 1D S-wave profile, all the profiles of one line or several parallel lines can be turned into a 2D or 3D image of the site using interpolation techniques, such as Kriging. Upcoming advanced inversion methods to determine S-wave velocity and the material damping ratio simultaneously or successively are described in Rix *et al.* (2000), Lai *et al.* (2002) and Badsar *et al.* (2010).

A MASW test consists of three steps. The first step involves the *in situ* experiment including vibration generation and the recording of seismic signals. The second step is the determination of the experimental dispersion curve by means of a frequency-wavenumber or phase velocity-frequency spectrum. If different modes appear and if they are sufficiently separated, mode specific curves can also be obtained. Finally, an inverse problem is formulated as an optimization problem between the experimental and computed theoretical dispersion curve.

Over the years a large number of inversion techniques have been proposed: fundamental mode inversion uses only the fundamental dispersion curve, while multi-mode inversion also incorporates higher modes and effective-mode inversion uses a dispersion curve that jumps with frequency from one mode to the other following the mode with the highest energy at a particular frequency. The concept of the effective dispersion curve was introduced to overcome the difficulty of numbering the modes properly. An overview of typical problems arising from dominating higher modes and recent inversion methods using the effective dispersion curve can be found in O'Neill and Matsuoka (2005). Zomorodian and Hunaidi (2006) presented an effective-mode inversion algorithm for the inversion of SASW data.

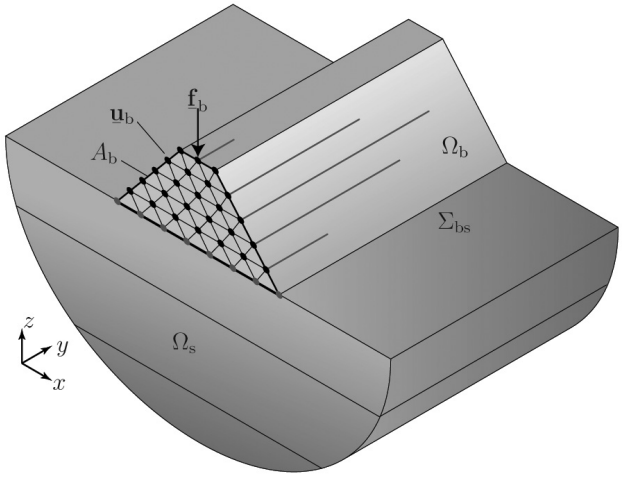

FIGURE 1
The geometry of the coupled soil-structure system.

THE APPLICABILITY OF SURFACE WAVE METHODS ON DYKES

Methodology of modelling

When MASW is employed to determine the dynamic soil characteristics of dykes, which have a 3D geometry, the pertinent question is under what conditions the known solutions of inversion for a layered and flat half-space will still be applicable leading to acceptable results.

In order to study this effect, a numerical analysis is performed to compare the dispersive wave propagation for different dyke geometries and material parameters with the results obtained in the flat-layered case. The numerical analysis fully accounts for the dyke geometry and the 3D wave propagation along the dyke.

As the dyke-soil system has a longitudinally invariant cross-section, a computationally efficient 2.5D approach can be applied (Aubry *et al.* 1994; Tadeu and Kausel 2000; François *et al.* 2010), where the Fourier transform of the longitudinal coordinate allows to represent the 3D response of the structure and the radiated wavefield on a 2D mesh. 2.5D boundary elements are used for the soil (Stamos and Beskos 1996; Sheng *et al.* 1999; Tadeu *et al.* 2002) while 2.5D finite elements are used for the dyke (Gavrić 1994, 1995). A number of examples of this approach have been presented by Sheng *et al.* (1999) for the computation of tunnels and railway tracks. Andersen and Nielsen (2005) and Andersen and Jones (2006) applied the methodology to study the effect of vibrating isolating screens along a railway track. A similar approach was followed by Lombaert *et al.* (2000, 2006) to predict vibrations induced by road and railway traffic.

The 2.5D methodology is used to compute the vertical displacements along the dyke crest due to a vertical harmonic point load on top of the dyke in the frequency-wavenumber domain (k_y, ω). This directly results in the phase velocity/frequency spectra, where the phase velocity V_y of waves propagating in the y-direction is related to the wavenumber as $V_y = \omega/k_y$. Subsequently, the dispersion curve is obtained for each frequency at the velocity at which the spectrum reaches its maximum.

Numerically, the dynamic soil-structure interaction problem is decomposed into two subdomains: the structure Ω_b and the semi-infinite layered soil Ω_s (Fig. 1). The dynamic soil-structure interaction problem is solved by enforcing continuity of displace-

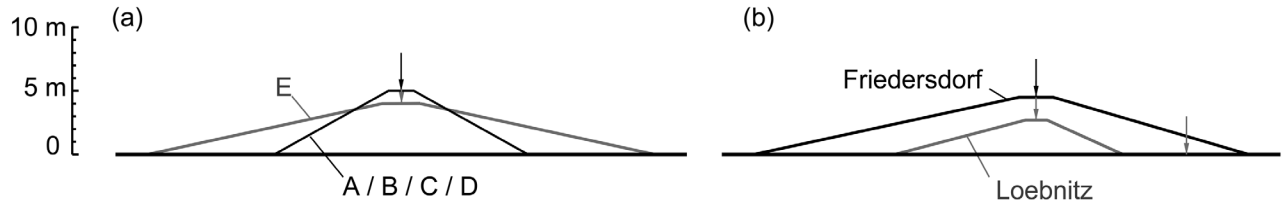

FIGURE 2
Scaled sketch of the dyke cross-sections: a) modelled and b) at test sites. Arrows indicate the location of the profiles.

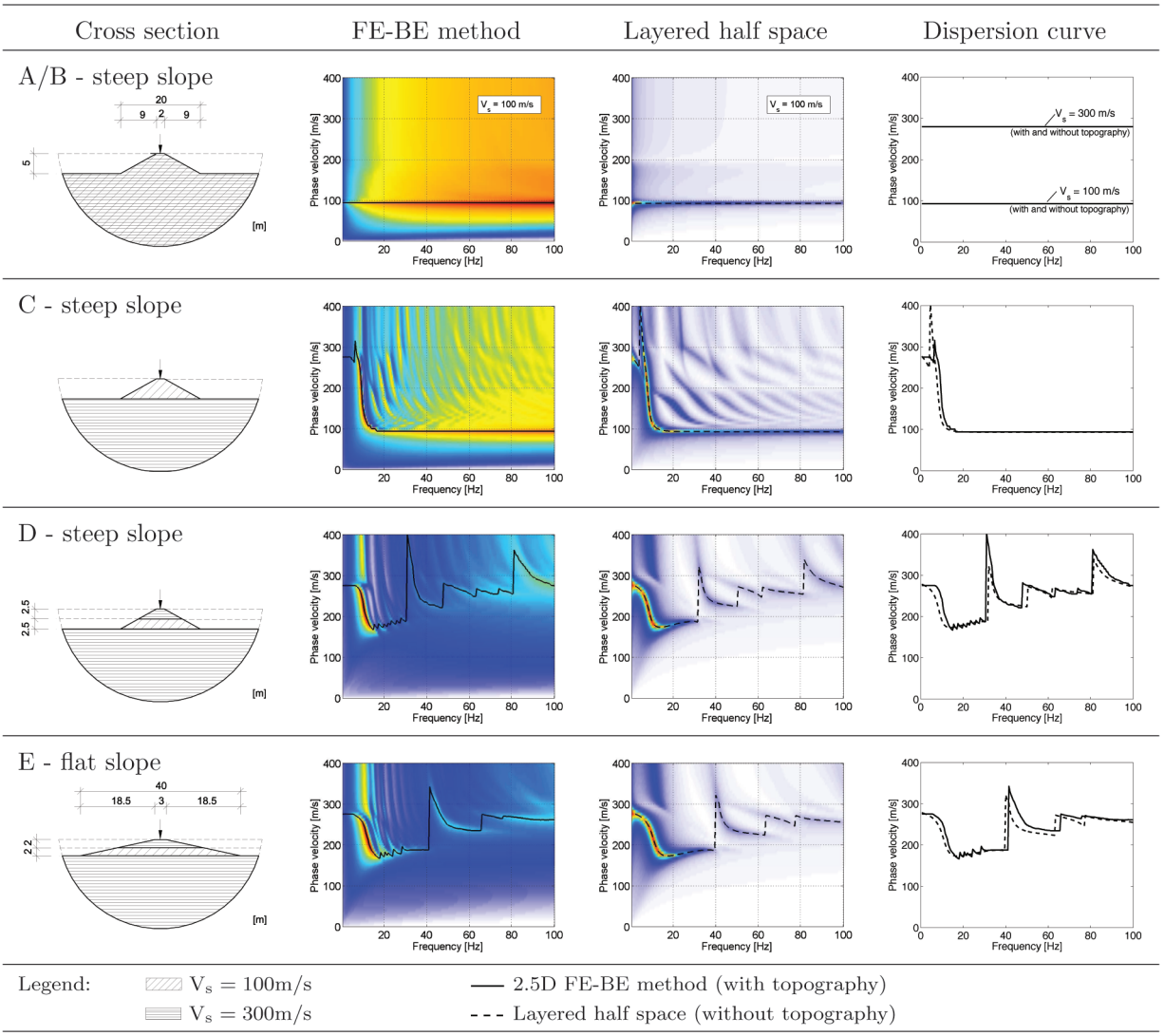

FIGURE 3
Phase velocity/frequency spectra and effective dispersion curve based on the FE-BE method and layered half-space model.

ments and equilibrium of stresses on the interface Σ_{bs} between both subdomains. Section A_b of the structure is invariant with respect to the longitudinal coordinate *y*. The dynamic soil-structure interaction problem is assumed to be linear and all equations are elaborated in the frequency domain. The dynamic equilibrium equation of the structure is discretized by means of 2.5D finite elements. The structure is considered as a 3D continuum and can be modelled with 2.5D volume elements.

As the structure is longitudinally invariant and has an invariant cross-section A_b, the displacement vector $\mathbf{u}_b(\mathbf{x}, \omega)$ is discretized as:

$$\mathbf{u}_b(\mathbf{x},\omega) \simeq \mathbf{N}_b(x,z)\underline{\mathbf{u}}_b(y,\omega), \quad (1)$$

where $\mathbf{N}_b(x, z)$ are the globally defined shape functions defined over the section A_b and $\underline{\mathbf{u}}_b(y,\omega)$ is the vector with degrees of freedom at all nodes of the two-dimensional mesh. x, y, z are the axes of the system according to Fig. 1. ω represents the circular frequency $2\pi f$ with the frequency f.

After application of the virtual work equation on the structure, the following discretized equilibrium equation is obtained:

$$\left[-\omega^2\mathbf{M}_{bb} + \mathbf{K}^0_{bb} - ik_y\mathbf{K}^1_{bb} - k_y^2\mathbf{K}^2_{bb} + \mathbf{K}^s_{bb}\left(k_y,\omega\right)\right]\underline{\tilde{\mathbf{u}}}_b\left(k_y,\omega\right) = \underline{\tilde{\mathbf{f}}}_b\left(k_y,\omega\right), \quad (2)$$

where a Fourier transform $\mathcal{F}\left[f(y),k_y\right] = \int_{-\infty}^{\infty}\exp\left(+ik_y y\right)f(y)\,dy$ of the longitudinal coordinate y to the horizontal wavenumber k_y has been performed. The matrices $\mathbf{M}_{bb}$ and $\mathbf{K}^0_{bb}$ correspond to the classical 2D finite element mass and stiffness matrices, respectively. The matrices $\mathbf{K}^1_{bb}$ and $\mathbf{K}^2_{bb}$ are stiffness matrices that account for the dependency on the wavenumber k_y. The vector $\underline{\tilde{\mathbf{f}}}_b\left(k_y,\omega\right)$ represents the external load on the structure. The matrix $\mathbf{K}^s_{bb}(k_y, \omega)$ in equation (2) is the stiffness matrix of the soil and is computed with a 2.5D boundary element method. As input for the boundary element model, the 2.5D Green's functions for a layered half-space are evaluated by means of the direct stiffness method (Kausel and Roësset 1981; Kausel 2006; Schevenels *et al.* 2009). As the free surface of the layered half-space is included in the fundamental solutions, the boundary element mesh can be limited to the interface between the structure and the soil. To simplify the finite element-boundary element coupling procedure, the boundary element mesh is chosen to correspond to the finite element mesh on the soil-structure interface.

Dispersion curves of dykes with different geometries and stiffness distributions

According to the dyke cross-sections tested in the frame of the later described survey campaign two symmetric geometries are selected. They mark the extremes of the dyke geometries at the sites (steep dyke versus flat dyke). Figure 2 shows the modelled and observed cross-sections. Characterizing for the first type of dyke is a slope angle of 56% (steep slope) and a crest height of 5 m; the second dyke has a slope angle of 21.5% (flat slope) in combination with a crest height of 4 m. The wave propagation is exemplarily studied for different layer configurations. Figure 3 shows the modelled dyke geometries and their parameters in the first column. The second and third columns of the figure give the phase velocity/frequency content of the modulus of the vertical displacement along the surface of the dyke due to a vertical force at the top. The resulting dispersion curves are displayed in column four. Poisson's ratio ν = 1/3, density ρ = 2000 kg/m^3 and material damping ratio D = 2% are kept constant.

Configurations A and B

Configurations A and B present a homogeneous dyke with an S-wave velocity of 100 m/s and 300 m/s, respectively. The resulting dispersion curves based on the model taking the topography into account coincide with the calculation for the homogeneous half-space. The dyke topography has no influence on the dispersion curves in this case. The Rayleigh wave velocity has a value of about 93.3% of the S-wave velocity agreeing with the expectations for a Poisson's ratio of 1/3.

Configuration C

This configuration is characterized by a soft dyke body (V_s = 100 m/s) overlaying a stiffer dyke base (V_s = 300 m/s). At frequencies smaller than about 9 Hz, the dispersion curves of both models show a phase velocity corresponding to the Rayleigh wave velocity of the underlying half-space. For frequencies above around 20 Hz the phase velocity approaches the Rayleigh wave velocity of a half-space with the properties of the dyke body. A remarkable peak appears in the transition zone at about 9–10 Hz. In the range of this peak a large part of the spectral energy shifts to a higher propagation mode and falls back afterwards to the fundamental mode. This phenomenon becomes clearer when viewing the fundamental mode and the first mode in the phase velocity/frequency plot of the layered half-space model. However, in the transition zone the dispersion curves of the layered half-space and the FE-BE model also show close proximity.

Configurations D and E

Configuration D shows a case where the dyke body contains a soft layer (V_s = 100 m/s) embedded in a stiff top layer and a stiff dyke base (V_s = 300 m/s). Configuration E is similar to D except that the dyke cross-section is of the second type characterized by a less steep slope. The effective dispersion curves start as in the previous example with a phase velocity corresponding to the half-space Rayleigh velocity of the dyke base and change afterwards in the frequency range between 5–15 Hz to lower velocities. However, the response is not dominated by the fundamental mode in most parts of the frequency range but by a number of higher order dispersive modes. Jumps appear in the dispersion curves of the FE-BE model at frequencies where the main wave energy shifts from one mode to another. For the layered half-space model, similar jumps in the effective dispersion curve are observed.

The dispersion curves resulting from the FE-BE model and layered half-space model show for both configurations, case D and E, great similarities. However, some differences can be noted as well. The transition of the dispersion curves from the half-space velocity to lower velocities takes place at slightly different frequencies. In case of the layered half-space model, the transition starts about 2 Hz before the beginning of the transition can be seen in the FE-BE model. A similar shift between the dispersion curves of the layered half-space and FE-BE model appears between 40–65 Hz in configuration E. In this range a higher mode is dominant and again the dispersion curve of the layered half-space model is shifted about 3–5 Hz towards lower frequencies in comparison to the FE-BE model.

Between 15–30 Hz, in which the fundamental mode is dominating, the dispersion curves resulting from the FE-BE model are

not fully smooth: instead characteristic ripples appear. By looking at the corresponding spectra the origin of the ripples becomes clearer. The dispersion curves in this frequency range are not the result of a single, continuous ridge in the spectra but of several smaller, almost vertical ridges that run parallel to each other. The effective dispersion curve sticks, according to its definition, strictly to the global maxima of the spectra leading to the observed discontinuities in the dispersion curves noticed as ripples.

The differences between the dispersion curves of the two models are qualitatively similar for configurations D and E. An inversion based on a layered half-space model will result in a comparably good approximation of the initially modelled layering. A variation of the slope angle in the range between the values of configuration D and E will most likely have no influence on the question of the applicability of the layered half-space model.

Conclusions for the testing campaign

The results of the forward modelling give an indication that the use of the layered half-space model is sufficiently accurate for the modelled cases of flat and steep dyke slopes. This seems to be true for stratifications with a normal layering but also for cases where a soft layer is embedded in stiffer material. Since the dykes at the test sites have in most cases a similar height, slope angle, toe width and top width compared to the modelled cross-section of configuration E (flat slope) a processing procedure based on a layered half-space model seems to be acceptable and was therefore used in the field test described later.

However, the comparison of FE-BE and the layered half-space model has so far only been performed on the level of the dispersion curves. The effects of small changes in the dispersion curve on the S-wave profile as a result of the inversion have not

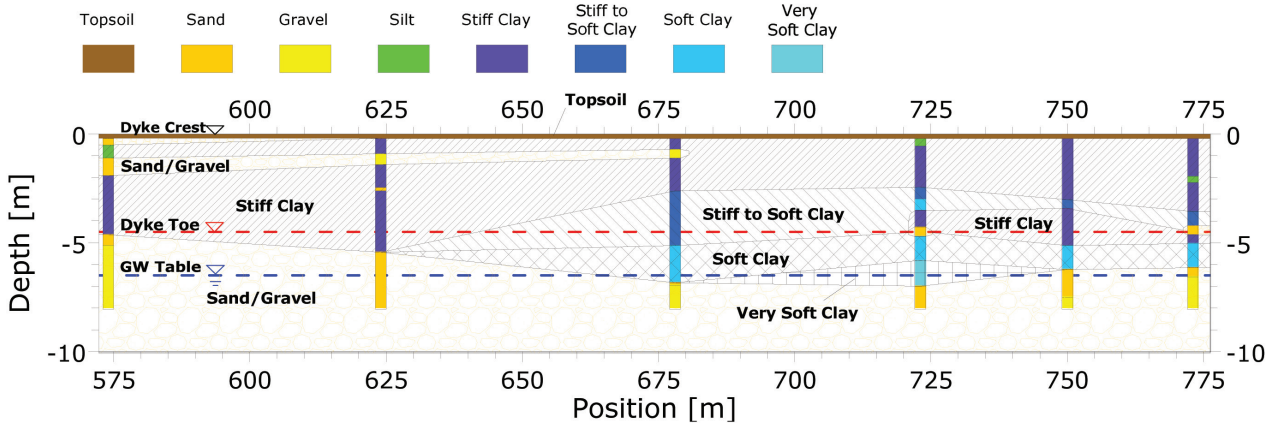

FIGURE 4

Longitudinal section through the crest of the dyke in Friedersdorf: stratification based on borehole data.

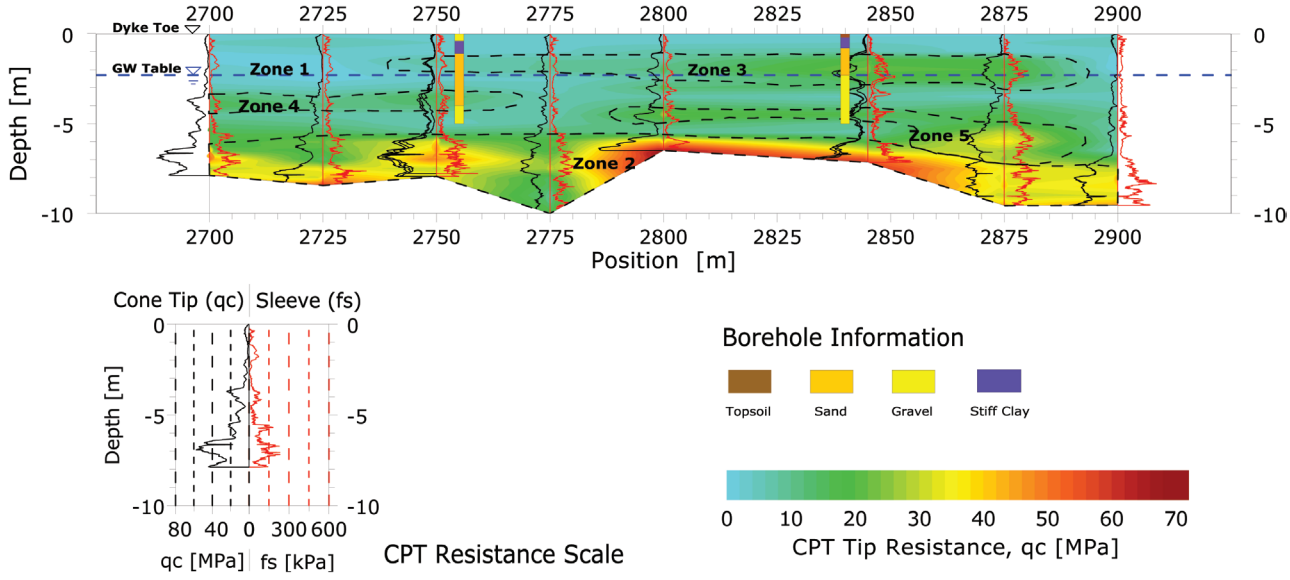

FIGURE 5

Longitudinal section in 5 m distance from the dyke toe in Loebnitz: interpreted cone penetration test profiles.

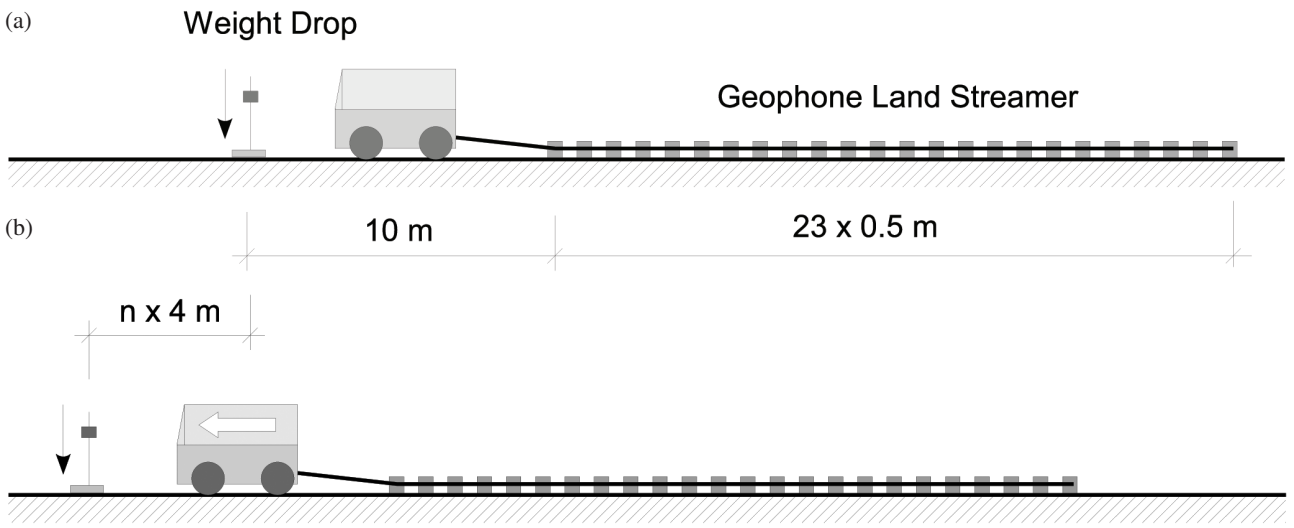

FIGURE 6
a) Test set-up and b) test progression along the measuring line.

been studied at this state. Therefore a comparison on the level of the inversion results at a single section of the real dyke will be discussed after presenting the results of the testing campaign.

The study also showed that under certain conditions the fundamental mode of the Rayleigh wave is not dominant. The inversion of soil profiles where higher modes are found in the experimental data requires the use of a forward model based on the effective dispersion curve or a procedure to separate the fundamental mode from other modes. The latter was applied while performing the data processing of the testing campaign.

DESCRIPTION OF THE TESTING SITES

The dyke sites investigated in July 2006 are situated on the river Mulde, near Bitterfeld, Germany. Two sections of the dyke were considered: the first is located in the community area of Friedersdorf and the second is situated in Loebnitz.

The dyke section in Friedersdorf is about 40 m wide at the dyke toe, 2.7 m wide at the crest and about 4.5 m high. The dyke has a slope of about 29% at the side pointing towards the river and approximately 21.5% on the other side. Available information from boreholes drilled at the crest showed that the core of the dyke consists of clay of varying consistency, whereas the base of the dyke is formed by gravel and sand. Figure 4 gives an interpretation of the layering based on the borehole descriptions. The MASW measurements were carried out along the centre line of the crest. The profile length was 200 m.

The dyke in Loebnitz is smaller but steeper: about 18 m wide at the dyke toe, 1.7 m wide at the crest, about 2.7 m high, with a 25% slope angle on the river side and 45% on the other side. A few available drilling logs show that the dyke body consists, in general, of clay that becomes softer in proximity to the groundwater table. The clay material changes to sand and gravel at a depth of about 1 m below the dyke toe.

A 200 m long MASW line was set up along the crest. Additionally, a MASW has been performed at a distance of 5 m from the dyke toe at the landside. While the dyke geometry has little influence on the MASW results on this line, it is selected because a large number of cone penetration test results is available from a previous measurement campaign.

The cone penetration test profiles were analysed in order to obtain information on the subsoil layering. The interpretation is based on the values for the cone tip resistance (q_c). For comparison, cone penetration test locations were 2D interpolated using a Kriging algorithm (Fig. 5). It can be seen that the tip resistance increases quite suddenly at a depth of 6 m to values above 30 MPa (zone 2). Above this depth several thin layers characterized by higher resistances (zones 3, 4, 5) were observed showing values from 10–20 MPa. Zone 1 is regarded as the matrix surrounding the other zones. The matrix is characterized by tip resistances below 10 MPa.

CHARACTERIZATION OF THE TESTING SITE BY SURFACE WAVES

Test set-up

Seismic data were acquired using a towed land streamer assembled from 24 vertical geophones with a natural frequency of 4.5 Hz. A 30 kg weight drop was employed for excitation. The geophones were spaced every 0.5 m and the offset between the source and nearest geophone was 10 m. This concludes in a total receiver array length of 11.5 m. Shots were repeated every 4 m along the line. The whole set-up was moved and the source-receiver offset was kept constant (Fig. 6). A total of 51 seismic records were acquired for later MASW processing.

According to the findings of O'Neill *et al.* (2008), the maximum lateral resolution of the set-up is equal to the half of the receiver array length, which means about 6 m. This needs to be kept in mind when interpreting the results.

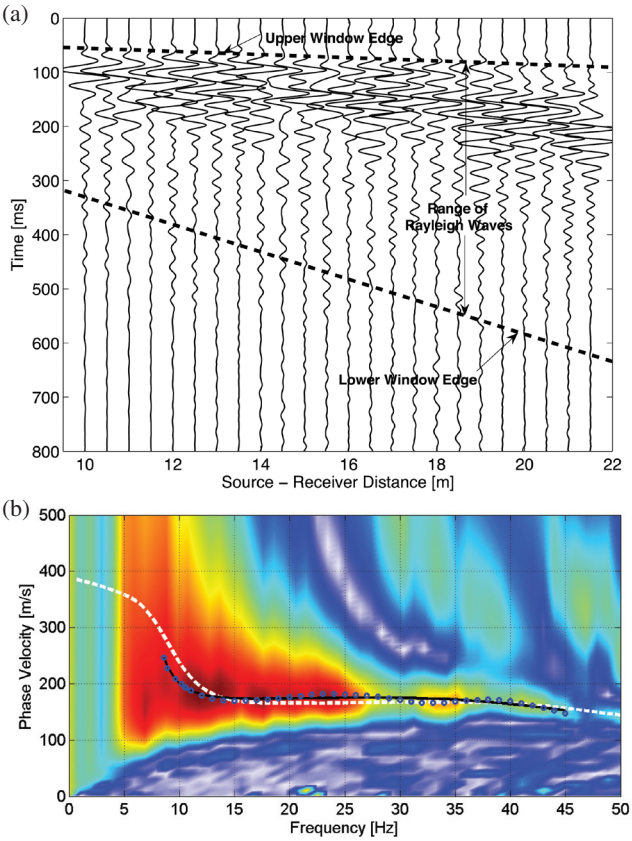

FIGURE 7
Friedersdorf, dyke crest, position 624 m: a) seismic record and b) frequency content, measured dispersion curve (blue circles), achieved fit after inversion (solid line), calculated curve by the FE-BE method (white dashed line).

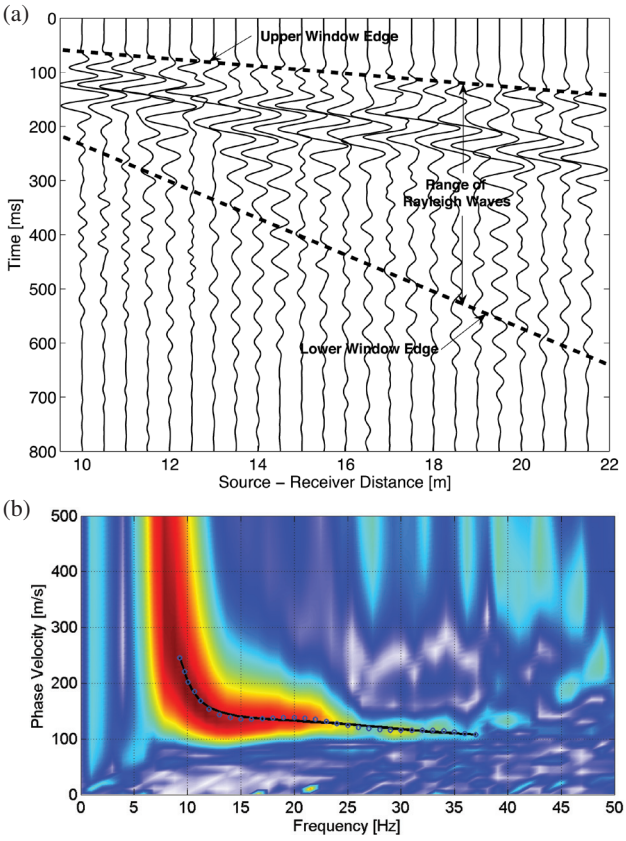

FIGURE 8
Loebnitz, dyke crest, position 2724 m: a) seismic record and b) frequency content, measured dispersion curve (blue circles), achieved fit after inversion (solid line).

Data processing

The gathered seismic data were processed and inverted using SurfSeis, a software package developed by the Kansas Geological Survey (Park *et al.* 1999). A multichannel window technique that mutes the interfering P-waves and noise components in the shot records (offset-time domain) was used to improve the range and resolution of the multimodal dispersion curves in the phase velocity/frequency domain (Ivanov *et al.* 2005). An example record for each measuring line with the boundaries of the manually adjusted muting windows can be found in Figs 7(a), 8(a) and 9(a). The muting improved the quality of the phase velocity/frequency spectrum at low frequencies leading to an easier identification of the propagation modes.

The records gathered in the offset/time domain are transferred into the phase velocity/frequency domain by applying a discrete Fourier transform on the time axis and a discrete slant stack transform on the distance axis. The fundamental mode of the Rayleigh wave was identified in the resulting plots and its dispersion curves were picked (Figs 7b, 8b, 9b). No significant higher mode could be identified.

The applied inversion algorithm supports only the S-wave velocities as variable parameters during the optimization. This also requires that the layer thicknesses are kept constant. Therefore, a starting model with a rather high number of layers needs to be used. In this project a model of nine layers on a half-space was chosen. The layer thicknesses increase exponentially with depth and were selected without the use of *a priori* information from the site. Available borehole logs and cone penetration test profiles were reserved for a later evaluation of the results.

The depth of the half-space is set approximately to half of the longest acquired wavelength making sure that the dispersion curve still contains some information on the properties of the half-space. This meant for Friedersdorf a half-space depth of 12 m and for Loebnitz a depth of approximately 10 m.

The S-wave velocity was chosen using a rule of thumb derived from the steady state Rayleigh method. A depth of $2.5 \cdot \lambda_R$ was assigned to a S-wave velocity equal to $1.1 \cdot V_R$, with λ_R the length of the Rayleigh wave and V_R the phase velocity (Foti 2000). Several years of MASW testing practice have shown that an initial model that takes the experimental dispersion curve into account improves the achieved curve fit after inversion and

results in more reliable S-wave velocity profiles than assuming a homogeneous or an arbitrary gradient medium.

The numerical forward algorithm is very insensitive to changes of the P-wave velocity and the density. Therefore, the initial P-wave velocity profiles were calculated from the S-wave profiles assuming a constant Poisson's ratio of 0.40 and the material density was set to 2000 kg/m^3 for all layers.

Each of the 200 m long survey profiles resulted in 51 1D V_s/depth plots. These were compiled into a 2D longitudinal section of the dyke by applying an exponential Kriging method. Each 1D profile is associated with the centre point of the geophone array. Examples of 1D S-wave profiles are shown in Fig. 10. An additional lateral low-pass filter aiming to reduce the lateral variation of the velocities was not used. Nevertheless, a slight smoothing effect is introduced due to the spacing between the grid points that was set to 2 m on the horizontal axis and to 1 m at the vertical axis. However, the small degree of smoothing by the Kriging is negligible compared to the smoothing caused by the 1D inversion itself.

Test results

Dyke Friedersdorf

The obtained 2D MASW section of the S-wave velocity is shown in Fig. 11. In the range from dyke position 620 m until the end of the survey line at 775 m three characteristic layers can be identified: 1) from the surface down to a level of about –3.5 m a layer with velocities between 185–230 m/s, 2) from –3.5 m to –6.5 m a layer with low velocities between 125–170 m/s and 3) a layer with higher velocities beginning with 200 m/s at –6.5 m and reaching 300 m/s at –10 m. At dyke positions smaller than 620 m the low velocity layer is not always present. At a few positions, i.e., at 585 m, 600 m, 625 m, 666 m, 677 m and 712 m, small areas with low velocities can be distinguished close to the surface of the dyke. Considering the spacing of shot points of 4 m it is clear that these low velocity areas appear only at single 1D profiles and are therefore not completely trustworthy. If the MASW results are compared with the longitudinal section

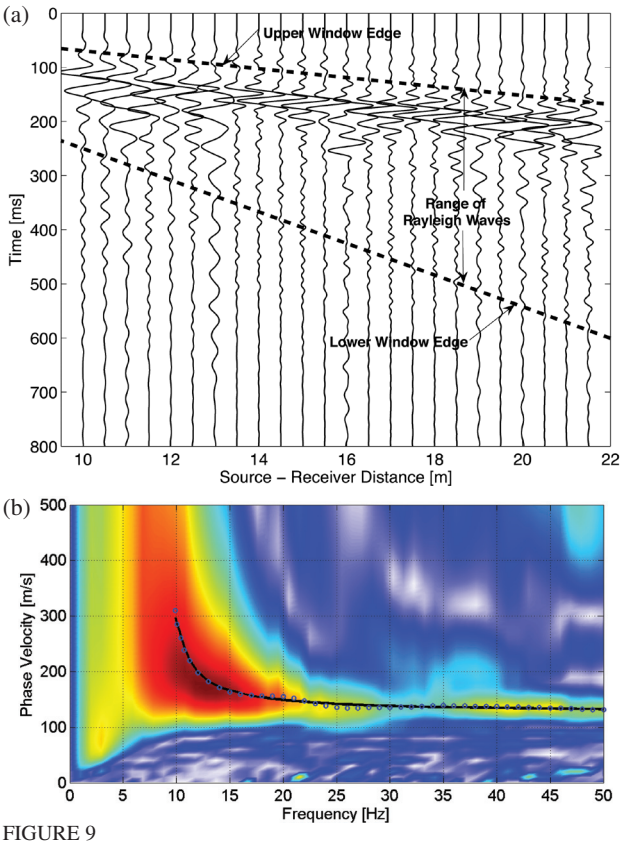

FIGURE 9

Loebnitz, dyke toe, position 2724 m: a) seismic record and b) frequency content, measured dispersion curve (blue circles), achieved fit after inversion (solid line).

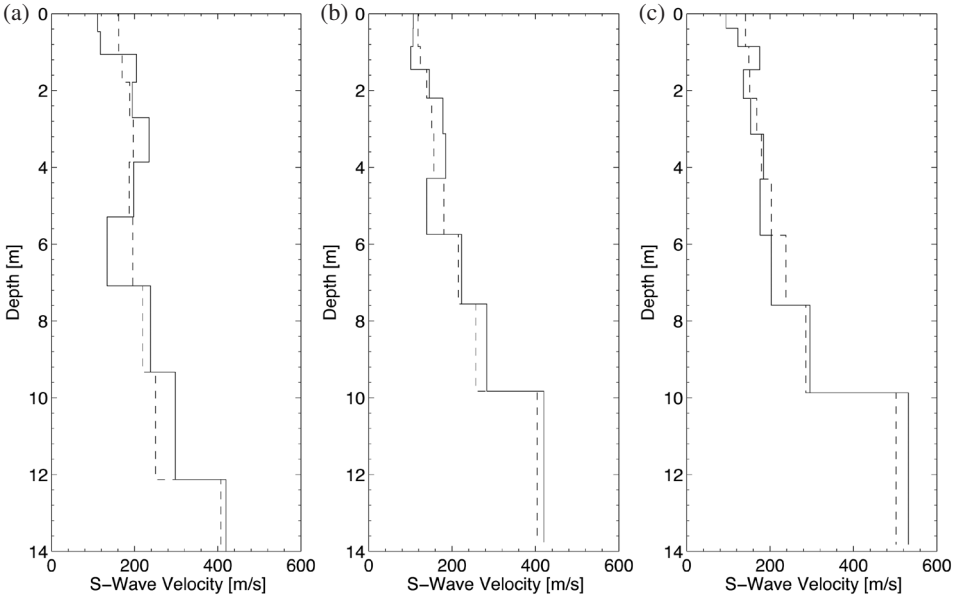

FIGURE 10

S-wave velocity profiles: a) dyke crest in Friedersdorf (position 624 m), initial profile (dashed line), inverted profile (solid line), b) dyke crest in Loebnitz (position 2724 m) and c) dyke toe in Loebnitz (position 2724 m).

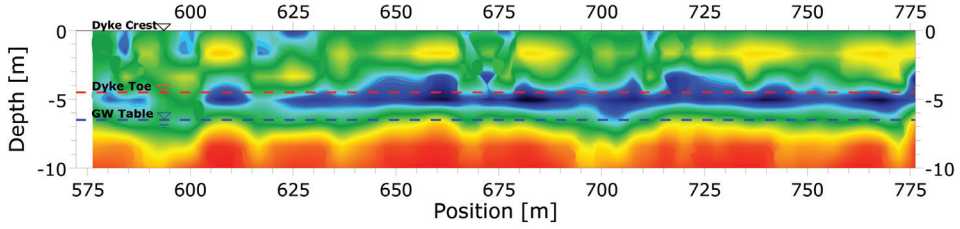

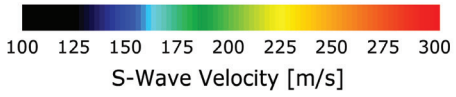

FIGURE 11
Longitudinal section through the crest of the dyke in Friedersdorf: S-wave velocities based on 51 vertical MASW profiles.

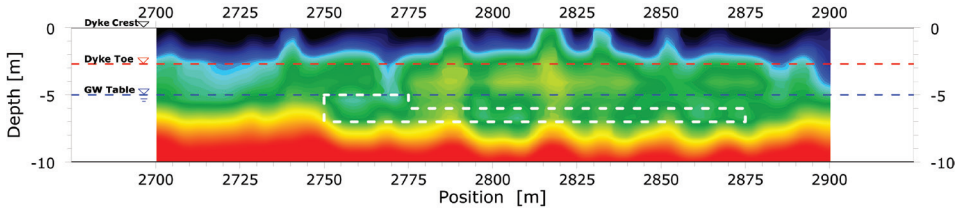

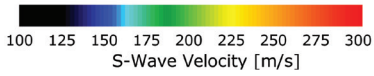

FIGURE 12
Longitudinal section through the crest of the dyke in Loebnitz: S-wave velocities based on 51 vertical MASW profiles, velocity inversion zone indicated by white dashed line.

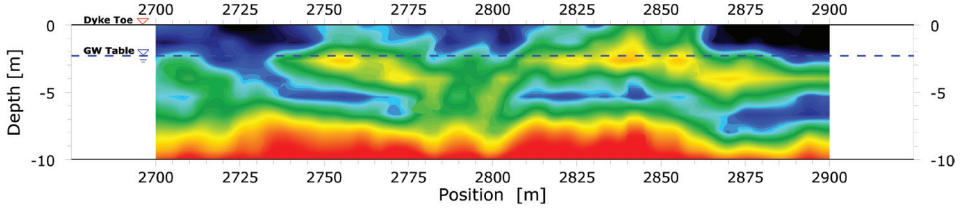

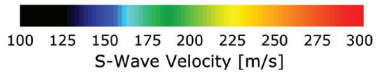

FIGURE 13
Longitudinal section in 5 m distance from the dyke toe in Loebnitz: S-wave velocities based on 51 vertical MASW profiles.

derived from the borehole descriptions it becomes obvious that the low velocity zone at the level of the dyke toe down to the groundwater table agrees quite well with the layer of soft and very soft clay in this depth and lateral extension.

Dyke Loebnitz (crest)

The MASW results along the dyke crest can be seen in Fig. 12. It shows materials with a low stiffness (V_s < 150 m/s) in the elevated part of the dyke. Below the dyke toe the velocity is increasing. The majority of 1D profiles between the positions 2750 m and 2875 m reveal a thin layer with a slight velocity inversion at depths between 6–7 m. In order to improve the visibility of this low velocity zone it has been marked in Fig. 12 by a white dashed line. Probably the same low velocity layer was identified in the later described MASW section at the landside of the dyke, more pronounced but slightly deeper (Fig. 13).

The uppermost 2 m of the dyke body are intersected at several positions, i.e., at 2740 m, 2787 m, 2816 m, 2852 m and 2831 m, by inclusions of materials with a slightly higher stiffness than measured in the surroundings. The phenomenon has similarities with the superficial low velocity zones found in the dyke in Friedersdorf. Also in this case the small singular velocity areas appear only in single 1D profiles. Therefore, the reliability of these zones needs to be considered as limited.

Unfortunately, at the dyke crest there was not such an elaborate drilling program performed as at the site in Friedersdorf. Besides, the dyke crest was not accessible by a cone penetration test vehicle. Therefore, an evaluation of the MASW results by means of comparison with other geotechnical parameters was not possible. Nevertheless, the quality of the seismic records and the calculated phase velocity/frequency spectra does not give an indication that the MASW results at the crest are less reliable than those gathered in Friedersdorf or at the dyke toe in Loebnitz. The latter are described in the following section.

Dyke Loebnitz (toe)

The 2D S-wave velocity profile at the dyke toe in Loebnitz can be found in Fig. 13. Below 7–8 m depth velocities above 220 m/s are dominant. The upper boundary of this area has a slight inclination towards the right end of the survey line. It is assumed that the

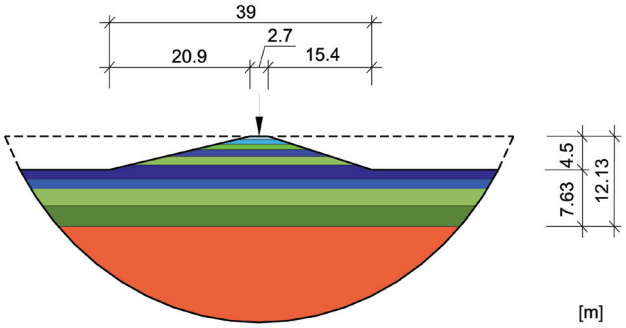

FIGURE 14
Geometry and material properties at position 624 m based on the inverted experimental dispersion curve, dyke in Friedersdorf.

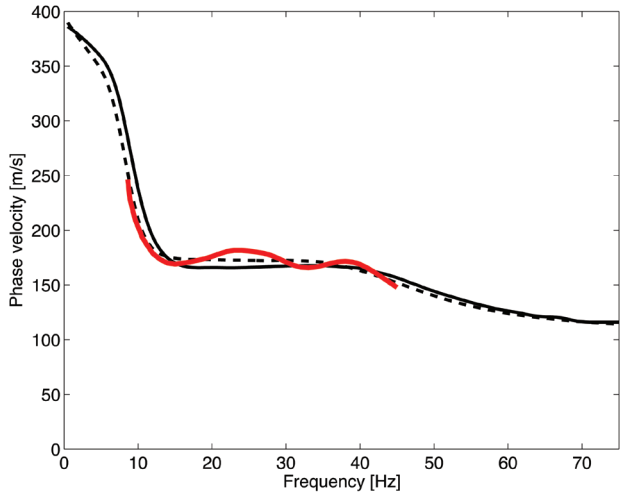

FIGURE 15
Fundamental dispersion mode at position 624 m, dyke in Friedersdorf; dyke FE-BE model (black solid line), equivalent half-space (black dashed line), measured (red solid line).

TABLE 1
Material properties at position 624 m based on the inverted experimental dispersion curve, dyke in Friedersdorf

Layer	Base depth (m)	V_s (m/s)	V_p (m/s)	Density (kg/m^3)
1	0.47	111.0	398.0	2000
2	1.06	117.1	398.0	2000
3	1.79	204.2	417.0	2000
4	2.71	194.0	460.0	2000
5	3.86	235.1	483.0	2000
6	5.29	197.6	459.0	2000
7	7.09	134.1	481.0	2000
8	9.33	238.2	537.0	2000
9	12.13	298.0	613.0	2000
HS	∞	419.7	997.0	2000

increasing velocity at this interface is not caused by a significant change of the sand material but simply by the mean effective stress gradually increasing with depth. The profile shows a thin layer of higher velocities (210–240 m/s) at depth levels between –2 and –4.5 m starting at around 2740 m towards the right end of the survey line. This layer is embedded in softer material with velocities lower than 160 m/s. The lower of the two low velocity layers found between 4–6 m depth is located slightly deeper compared to the most probable same low velocity layer found at the dyke crest (Fig. 12). Anyhow, this low velocity layer is more pronounced regarding thickness and velocity drop. The differences between the crest and toe section concerning the inversion

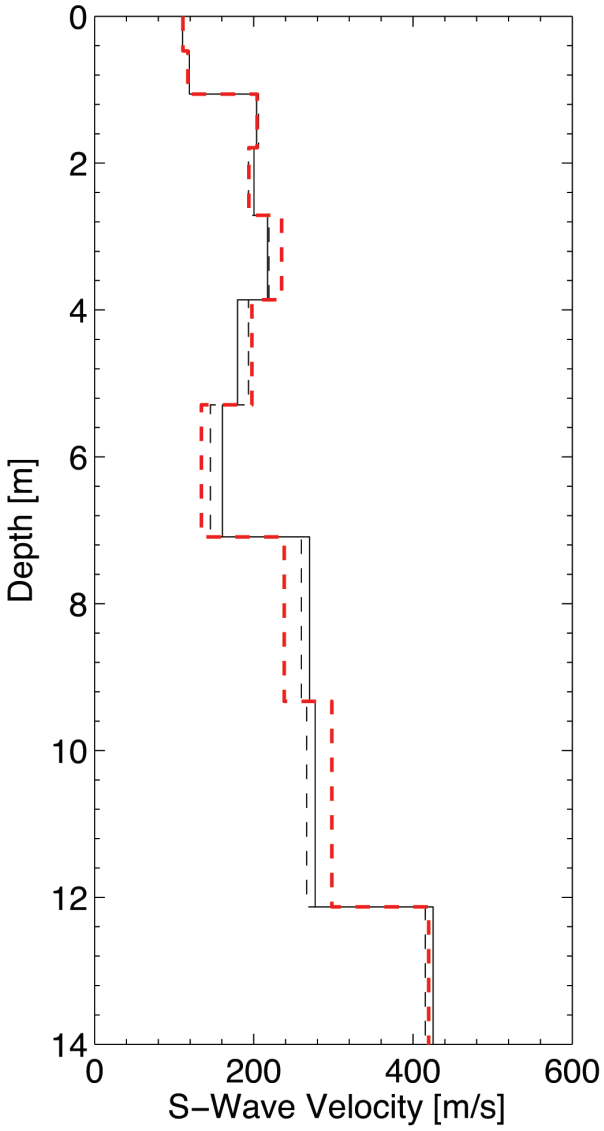

FIGURE 16
S-wave velocity profiles: layered half-space inversion of numerically modelled dispersion curves (Friedersdorf), FE-BE model (solid line), layered half-space model (dashed line), in comparison to modelled profile (red dashed line).

zone could be due to the different overburden pressure, which should be higher at the crest at the same elevation.

Remarkably, small areas with velocities below 120 m/s are present at several positions close to the surface.

Looking at the cone penetration test tip resistances (Fig. 5) it can be seen that zones 2 and 3 correspond reasonably well with the higher S-wave velocities. Zone 4 and especially zone 5 cannot be resolved in the velocity profile. It is assumed that this is due to limitations of the MASW method in identifying such thin inclusions.

Model of a cross-section at the dyke in Friedersdorf with true surface topography

In order to substantiate our conclusion that the half-space model could be used on dyke structures, a typical cross-section of the dyke at Friedersdorf was selected aiming to compare the FE-BE model and half-space model based on real dyke geometry. Figure 14 shows a sketch of the dyke cross-section in Friedersdorf at position 624 m. The material parameters of this section and layer boundaries, both given in Table 1, were taken from the results of the MASW inversion with SurfSeis. The dispersion curves were calculated using the FE-BE and the equivalent layered half-space model. The results showing the fundamental modes are given in Fig. 15. The two dispersion curves of the FE-BE and layered half-space method agree very well. This is an indication that for the selected geometry and material parameters wave propagation can be sufficiently described by a layered half-space model. In Fig. 7(b) the calculated FE-BE curve overlaid on the phase velocity/frequency spectrum of the measured data at the same position is shown.

Figure 16 displays the S-wave profiles obtained from inverting the modelled dispersion curves, FE-BE method versus layered half-space, using SurfSeis based on the dyke model (Fig. 13). The depth of the half-space was set to about 12 m. S- and P-wave velocities of the start profile were chosen according to the same rule applied to the measured data. The density was set to 2000 kg/m^3 and the Poisson's ratio to 0.40 again. The number of layers and their thicknesses agree with the originally modelled profile (Fig. 14 and red dashed line in Fig. 16). The two S-wave profiles obtained approximate reasonably well the originally modelled profiles. A significant difference between the calculated profiles could not be observed. The good agreement, also on the level of S-wave velocities, supports our previous assumption of using a 1D layered half-space even in the case of dyke topography.

CONCLUSIONS

MASW surveys on two sections of a river dyke were presented and a numerical model was used to study the wave propagation along the real geometry. The numerical model accounts fully for the elevated dyke topography. The survey lines were placed once directly on the crest of the dyke and once along the dyke toe.

The numerical study shows the validity of a layered half-space model for MASW inversion for the studied dyke geometries. This includes dykes with a base width-to- height ratio larger than four. Even in the case of an embedded low velocity layer almost no difference between the dispersion curves of the layered half-space model and the FE-BE dyke model was observed. However, steeper dykes were not studied, due to their missing relevance for the testing campaign. These dykes may cause problems if the layered half-space model is employed and should be subjected to further research.

The results of the MASW field tests were compared with the core description of boreholes on a site in Friedersdorf and with the results of cone penetration tests near a dyke in Loebnitz. Several layers of different dynamic stiffness could be identified. A remarkable correlation between the consistency of the clay material in the core of the Friedersdorf dyke and the S-wave velocity was found: low velocities (125–170 m/s) correspond with soft and very soft clays; stiff clays show higher velocities (185–230 m/s). Locations of weak material close to the surface could be marked.

The longitudinal section through the dyke crest in Loebnitz reveals in parts of the section a thin layer with a velocity inversion at depths between 6–7 m. A similar but deeper inversion zone is found at the place of the longitudinal section on the dyke toe and also in the cone penetration test profiles from the dyke toe.

The findings from the survey line near the dyke toe in Loebnitz cannot contribute to the question whether the use of a layered half-space as a forward model is valid or not. This is due to the fact that the dyke geometry does not significantly affect the MASW measurement beside the dyke. On the other hand, at this line a number of cone penetration test profiles were available. Since the cone penetration test data have a very high vertical resolution, even better than one can expect from the drilling logs at the Friedersdorf site, the comparison to the MASW results can provide important information on the performance of the MASW method concerning its ability to resolve soils with a high structural heterogeneity.

As expected the measured S-wave velocity corresponds to the cone penetration test resistance in Loebnitz; layers with high tip resistances agree with layers of high S-wave velocity and vice versa. However, the resolution of the MASW method was found to be not sufficiently high to resolve all the features of the very detailed cone penetration test profiles. This makes it questionable if the method will be able to identify small size inclusions (dimensions: 1–2 m) with increased hydraulic conductivity such as sand and gravel pockets providing the path for dangerous erosion and seepage processes. However, a general trend of the structural changes along the dyke can be obtained. The results can be used to guide a later testing campaign using direct probing techniques.

ACKNOWLEDGEMENTS

The results presented in this work were obtained within the frame of the BMBF-project DEISTRUKT (No. 02WH0639). The financial support of the German Ministry for Education and Research is

gratefully acknowledged. The third and fourth authors are holders of a Postdoctoral Fellowship of the Research Foundation-Flanders (FWO-Vlaanderen). The financial support of FWO-Vlaanderen is kindly acknowledged. Special thanks go to the Department of Monitoring and Exploration Technologies at the Helmholz Centre for Environmental Research Leipzig (UFZ) for providing the cone penetration test results and to Planungsgesellschaft Scholz + Lewis mbH Dresden for the borehole data.

REFERENCES

Al-Hunaidi M.O. 1996. Nondestructive evaluation of pavements using spectral analysis of surface waves in the frequency wave-number domain. *Journal of Nondestructive Evaluation* **15**, 71–82.

Andersen L. and Jones C.J.C. 2006. Coupled boundary and finite element analysis of vibration from railway tunnels – A comparison of two- and three-dimensional models. *Journal of Sound and Vibration* **293**, 611–625.

Andersen L. and Nielsen S.R.K. 2005. Reduction of ground vibration by means of barriers or soil improvement along a railway track. *Soil Dynamics and Earthquake Engineering* **25**, 701–716.

Aubry D., Clouteau D. and Bonnet G. 1994. Modelling of wave propagation due to fixed or mobile dynamic sources. In: *Workshop Wave '94, Wave Propagation and Reduction of Vibrations* (eds N. Chouw and G. Schmid), pp. 109–121. Ruhr University of Bochum.

Badsar S.A., Schevenels M., Haegeman W. and Degrande G. 2010. Determination of the material damping ratio in the soil from SASW tests using the half-power bandwidth method. *Geophysical Journal International* **182**, 1493–1508.

Donié C., Krajewski W. and Wawrzyniak C. 2007. Geoelektrisch-geotechnische Erkundung von Hochwasserschutzdeichen. *Geotechnik* **30**, 42–47 (in German).

Fauchard C. and Mériaux P. 2007. *Geophysical and Geotechnical Methods for Diagnosing Flood Protection Dikes – Guide for Implementation and Interpretation*. Éditions Quae.

Foti S. 2000. *Multistation methods for geotechnical characterization using surface waves*. PhD thesis, Politecnico di Torino.

François S., Schevenels M., Galvín P., Lombaert G. and Degrande G.A. 2010. 2.5D coupled FE-BE methodology for the dynamic interaction between longitudinally invariant structures and a layered halfspace. *Computer Methods in Applied Mechanics and Engineering* **199**, 1536–1548.

Gavrić L. 1994. Finite element computation of dispersion properties of thin-walled structures. *Journal of Sound and Vibrations* **173**, 113–124.

Gavrić L. 1995. Computation of propagative waves in free rail using finite element technique. *Journal of Sound and Vibrations* **183**, 531–543.

Gunn D.A., Nelder L.M., Chambers J.E., Raines M.G., Reeves H.J., Boon D.P., Pearson S.G., Haslam E.P., Carney J.N., Stirling A., Ghataora G.S., Burrow M.P.N., Tinsley R.D. and Tilden-Smith R. 2006. Assessment of railway embankment stiffness using continuous surface waves. *Proceedings of the 1st International Conference on Railway Foundations*, Birmingham, UK, Expanded Abstracts, 94–106.

Henning T., Weller A. and Canh T. 2005. The effect of dike geometry on different resistivity configurations. *Journal of Applied Geophysics* **57**, 278–292.

Ivanov J., Park C.B., Miller R.D. and Xia J. 2005. Analyzing and filtering surface-wave energy by muting shot gathers. *Journal of Environmental and Engineering Geophysics* **10**, 307–321.

Kausel E. 2006. *Fundamental Solutions in Elastodynamics: A Compendium*. Cambridge University Press.

Kausel E. and Roësset J.M. 1981. Stiffness matrices for layered soils. *Bulletin of the Seismological Society of America* **71**, 1743–1761.

Kramer S.L. 1996. *Geotechnical Earthquake Engineering*. Prentice Hall.

Lai C.G., Rix G.J., Foti S. and Roma V. 2002. Simultaneous measurement and inversion of surface wave dispersion and attenuation curves. *Soil Dynamics and Earthquake Engineering* **22**, 923–930.

Lane Jr. J.W., Ivanov J., Day-Lewis F.D., Clemens D., Patev R. and Miller R.D. 2008. Levee evaluation using MASW: Preliminary findings from the Citrus Lakefront Levee, New Orleans, Louisiana. *21st Symposium on the Application of Geophysics to Engineering and Environmental Problems*, Philadelphia, USA, Expanded Abstracts, 703–712.

Lombaert G., Degrande G. and Clouteau D. 2000. Numerical modelling of free field traffic induced vibrations. *Soil Dynamics and Earthquake Engineering* **19**, 473–488.

Lombaert G., Degrande G., Kogut J. and François S. 2006. The experimental validation of a numerical model for the prediction of railway induced vibrations. *Journal of Sound and Vibrations* **297**, 512–535.

Min D.-J. and Kim H.-S. 2006. Feasibility of the surface-wave method for the assessment of physical properties of a dam using numerical analysis. *Journal of Applied Geophysics* **59**, 236–243.

Nazarian S., Stokoe II K.H. and Hudson W.R. 1983. Use of spectral analysis of surface waves method for the determination of moduli and thickness of pavement systems. *Transportation Research Record* **930**, 38–45.

O'Neill A., Campbell T. and Matsuoka T. 2008. Lateral resolution and lithological interpretation of surface-wave profiling. *The Leading Edge* **27**, 1550–1563.

O'Neill A. and Matsuoka T. 2005. Dominant higher surface-wave modes and possible inversion pitfalls. *Journal of Environmental and Engineering Geophysics* **10**, 185–201.

Park C.B., Miller R.D. and Xia J. 1999. Multichannel analysis of surface waves. *Geophysics* **64**, 800–808.

Rix G.J., Lai C.G. and Spang A.W. 2000. In situ measurement of damping ratio using surface waves. *Journal of Geotechnical and Geoenvironmental Engineering* **126**, 472–480.

Schevenels M., François S. and Degrande G. 2009. EDT: An ElastoDynamics Toolbox for MATLAB. *Computers & Geosciences* **35**, 1752–1754.

Sheng X., Jones C.J.C. and Petyt M. 1999. Ground vibration generated by a harmonic load acting on a railway track. *Journal of Sound and Vibrations* **225**, 3–28.

Stamos A.A. and Beskos D.E. 1996. 3-D seismic response analysis of long lined tunnels in half-space. *Soil Dynamics and Earthquake Engineering* **15**, 111–118.

Stokoe II K.H. and Nazarian S. 1983. Effectiveness of ground improvement from spectral analysis of surface waves. *8th European Conference on Soil Mechanics and Foundation Engineering,* Helsinki, Finland, Expanded Abstracts.

Tadeu A.J.B., Antonio J.M.P. and Kausel E. 2002. 3D scattering of waves by a cylindrical irregular cavity of infinite length in a homogeneous elastic medium. *Computer Methods in Applied Mechanics and Engineering* **191**, 3015–3033.

Tadeu A.J.B. and Kausel E. 2000. Green's functions for two-and-a-half-dimensional elastodynamic problems. *ASCE Journal of Engineering Mechanics* **126**, 1093–1096.

Tuyen D.V., Canh T. and Weller A. 2000. Geophysical investigations of river dikes in Vietnam. *European Journal of Environmental and Engineering Geophysics* **4**, 195–206.

Xia J., Miller R.D. and Park C.B. 1999. Estimation of near-surface shear-wave velocity by inversion of Rayleigh waves. *Geophysics* **64**, 691–700.

Zomorodian S.M.A. and Hunaidi O. 2006. Inversion of SASW dispersion curves based on maximum flexibility coefficients in the wave number domain. *Soil Dynamics and Earthquake Engineering* **26**, 735–752.